Giant, 2, 2020, 100019

Short communication

Manipulating small water droplets on a photo-switchable mat of fluorinated linear liquid crystal polymers

Xiao Zhang[1], Lang Qin[1], Yuyun Liu, Jia Wei, Yanlei Yu*

Department of Materials Science and State Key Laboratory of Molecular Engineering of Polymers, Fudan University, Shanghai 200433, China

Keywords: Liquid crystal polymers, Tunable adhesive force, Azobenzene, Surface chemistry, Electrospinning

Manipulating small water droplets on an intelligent surface with tunable superhydrophobic adhesion has attracted considerable interests because of potential applications ranging from no-loss transfer to surface chemistry but remains challenging. Herein, we present a strategy to manipulate the small water droplet on a photo-switchable mat, which is fabricated by a fluorinated linear liquid crystal polymer via electrospinning. The electrospun mat with hierarchical microstructures exhibits fast and reversible superhydrophobic adhesion change, and still remains the superhydrophobicity after pinning and removing of the water droplets for several times. Diverse erasable and rewritable arrays on the vertically placed mat are formed by pinning the small water droplets to any high adhesive position after localized light irradiation. Moreover, after evaporation of the water droplets containing aggregation-induced emission materials, the mat exhibits bright fluorescence upon faint UV irradiation to indicate the trace with the same pattern as the original droplets. Such photo-switchable superhydrophobic mats would provide an open tunable surface for microdroplets manipulation.

1 Introduction

Discovery of intriguing wetting phenomena on the surface in nature have accelerated the development of artificial superwettability systems, which play important roles in many applications ranging from self-cleaning to liquid-liquid separation [1–5]. Recent research has focused on the intelligent surfaces with switchable wetting states in response to heat [6–8], pH [9,10], ion [11], and electric field [12]. Compared to these stimuli, the accessibility of remote, local, and spatial manipulation makes photo-responsive materials arouse intense interests of researchers [13–16]. Typically, superhydrophobic surfaces with hierarchically structure fabricated by semiconductor nanoparticles (e.g. zinc oxide or titanium dioxide) exhibit photo-induced superhydrophilicity, but require a relatively long time for their recovery process in dark [3]. Alternatively, organic and polymeric materials containing azobenzenes can rapidly undergo reversible photoisomerization between rod-like *trans* and bent *cis* isomers, which causes a change in dipole moment as well as surface wettability [17,18]. Jiang et al. fabricated a superhydrophobic azobenzene monolayer on the rough substrates through electrostatic self-assembly technique and realized a large reversible water contact angle (CA) change of about 66° upon UV and visible light irradiation [19]. By using the same technique, Cho et al. reported an erasable and rewritable nanostructured multilayer film that could be reversibly switched between

* Corresponding author.
E-mail address: ylyu@fudan.edu.cn (Y. Yu).
Received 15 June 2020; Received in revised form 22 July 2020; Accepted 23 July 2020
[1] Both the authors contributed equally to this work.

https://doi.org/10.1016/j.giant.2020.100019

superhydrophobicity (CA > 150°) and superhydrophilicity (CA < 5°) with the help of fluorinated azobenzene molecules and selective irradiation [20].

Few of these works, however, involved a method to fabricate intelligent surfaces with photo-switchable superhydrophobic adhesion, which are promising candidates to manipulate the motion of water droplets for no-loss transfer [21]. Azobenzene-containing liquid crystal polymers (LCPs) show superior in the fabrication of such surfaces because the *trans-cis* photoisomerization of azobenzene results in not only changes of surface energy, but also photochemical phase transition attributed to the cooperative effect of the LCs, and produces macroscale deformation of the LCPs [22–26]. We previously demonstrated in situ photo-induced switching of superhydrophobic adhesion on a microarrayed crosslinked LCP film, where the sliding angle (SA) was reversibly changed between 68° and 90° [27]. However, the crosslinked network of LCPs results in the difficulties in both modulation of hierarchical structure and fabrication of the surface with a large area. Recently, we have developed a novel class of azobenzene-containing linear LCPs (LLCPs) with high molecular weight, which possessed robust mechanical properties and were facilely constructed into 3-dimensional structures exhibiting excellent photodeformability [23,28]. Owing to their good processability (compatible with common solution and melt processing), a photoresponsive mat was fabricated from the LLCP by electrospinning and presented large superhydrophobic adhesion changes. Therefore, light-directed pinning of the moving water droplets (5–9 μL) has been realized at any desired position [29].

When the volume became smaller, water droplets are easily trapped in the structures, which leads to sticky Wenzel states and may destroy the superhydrophobicity of the surface [1]. Therefore, a water droplet $\leq$ 4 μL was stuck on the mat, indicating that manipulation of smaller droplets still remains challenging, which requires the LLCP of lower surface energy and multiscale surface structures on the mat.

Here, we demonstrate the manipulation of the 3 μL water droplets on the photo-switchable superhydrophobic mats, which are fabricated from a LLCP containing azobenzene and fluorinated alkyl chain by electrospinning. The LLCP mat is able to be reversibly switched between two completely different wetting states, like lotus leaves and rose petals, by UV (365 nm) and visible (530 nm) light irradiation (Fig. 1a). The 3 μL water droplet rolls off at the low adhesive state, while become pinned to the surface at the high adhesive state, even when the LLCP mat is turned upside down. Moreover, diverse arrays are programmed by pinning the water droplets to the localized areas exposed to UV light.

2 Methods

2.1 Synthesis of the monomer

4-((4-((11-hydroxyundecyl)oxy)phenyl)diazenyl)benzoic acid [30] (3 g, 7.3 mmol), 1′1′−2H-fluorine butanol (2.0 g, 10 mmol) and 4-dimethylaminopyridine (DMAP, 0.48 g, 0.4 mmol) were added into 500 mL flask and dissolved by 150 mL dichloromethane. Then, dicyclohexylcarbodiimide (DCC, 4.5 g, 20 mmol) in 60 mL dichloromethane was added dropwise into the mixture. After stirring at room temperature for 24 h, the mixture was filtrated to remove the precipitates. The orange solid product was obtained by column chromatography with silica gel using dichloromethane (3.02 g, 5.07 mmol, 70%) and used in the next step.

A mixture of orange product (1.78 g, 3 mmol), 4-(cyclooct-4-en-1-yloxy)−4-oxobutanoic acid (0.9 g, 4.0 mmol) and DMAP (4.8 g, 4 mmol) were stirred in 150 mL dichloromethane. The solution of DCC in 50 mL dichloromethane was added dropwise into the reaction mixture at 0 °C. After the mixture was stirred at room temperature for 24 h, the precipitate formed during the reaction was filtered off and the organic solution was washed with water. The organic phase was dried with magnesium sulfate and the solvent was removed. The crude product was purified by silica gel column chromatography using chloroform as the eluent and recrystallized from methanol to give the monomer (1.48 g, 1.85 mmol, 61%).

2.2 Polymerization of the LLCP

The polymerization was performed using standard Schlenk techniques under an argon atmosphere. The monomer (0.4 g, 0.5 mmol) was added into a Schlenk flask. Then, 0.5 μmol second-generation Grubbs catalyst with 2 mL anhydrous dichloromethane was added into the mixture. After stirring for 3 h at 45 °C, the yellow solid polymer was precipitated from methanol (0.37 g, 93%).

2.3 Electrospinning

The electrospun device is composed of a high-voltage supply (TPRXs Regulated DC power supply), a programmable syringe pump (TJ-1A Syringe Longer Pump) and a collection iron plate. The LLCP was dissolved in dichloromethane by stirring 1 h and ultrasonic treating to concentration of 0.5 wt%, 1 wt%, and 2 wt%, respectively. In an electrospinning unit, the LLCP solution was fed at a constant rate of 3 mL h^{-1} to a syringe by a digitally controlled micropump. The tip of the syringe was connected to a high-voltage supply. Electrospinning was carried out at an electrical potential of 16 kV using a needle with an inner diameter of about 0.6 mm. The distance between the needle tip and the grounded collector was fixed at about 15 cm. The electrospinning was carried out at room temperature. The mats were collected on iron plate for 10 min and then dried at room temperature for 12 h.

2.4 Characterization of the mats

The optical textures, morphology for the electrospun mats were observed by field-emission scanning electron microscopy (FESEM) (Zeiss, Ultra 55). The thermal characteristics of polymer LLCP were conducted by using a Modulated DSC (TA Instruments) in a nitrogen atmosphere. The mesomorphic properties of the parallel aligned mat was acquired by optical polarizing microscopy (POM) (Leica, DM2500P). The UV–vis spectra of diluted LLCP solutions was recorded by UV–Vis-NIR spectrophotometer (Pekin Elmer, Lambda 650). The number molecular weight of the LLCP was studied in THF by Gel permeation chromatography (GPC) (Agilent, 1260). Adhesive forces (AFs) measurements were performed on Dataphysics DCAT25. Two-dimensional wide-angle X-ray diffraction (2D-WAXD) experiments of the LLCP fiber were conducted on a small angle/wide angle scatterometer (Xeuss

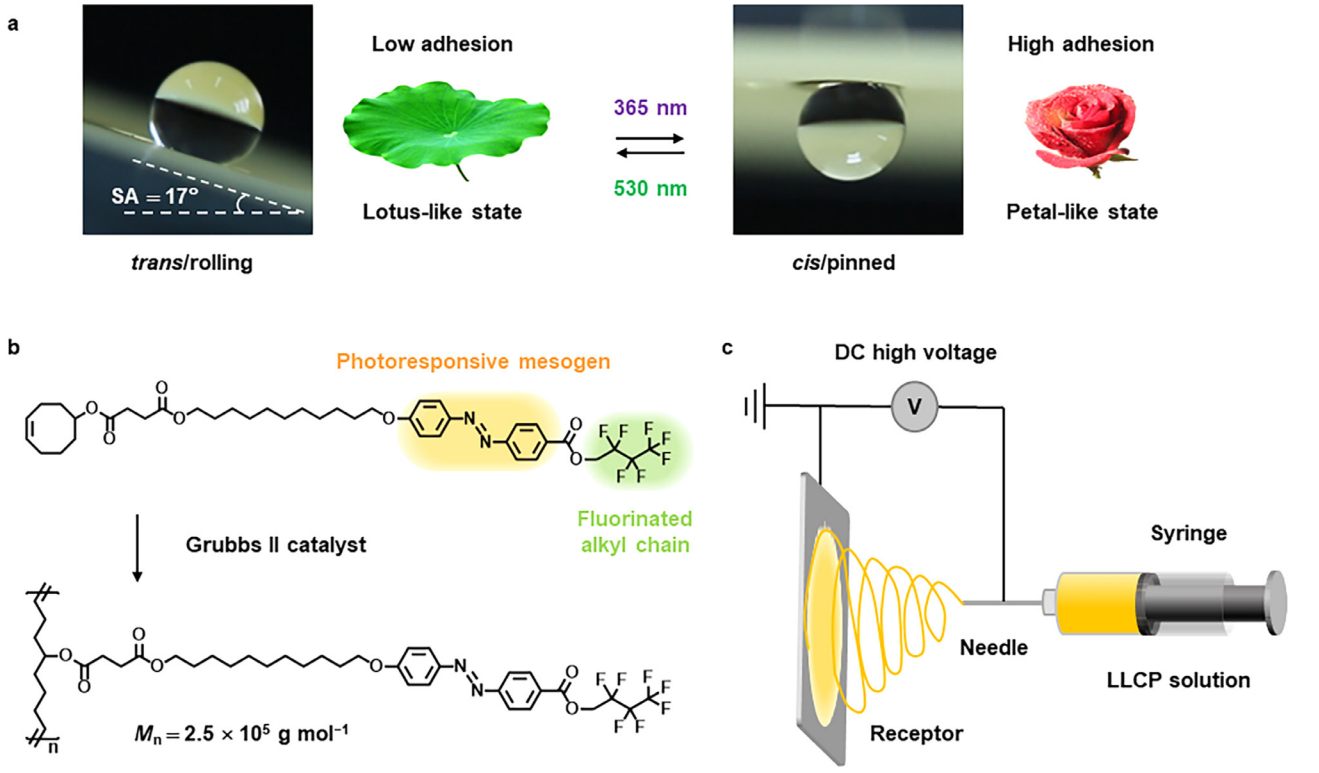

Fig. 1

(a) Photographs to show the reversible switching of the superhydrophobic LLCP mat between low adhesion state (left) and high adhesion state (right) by light. A 3 μL water droplet rolls off the surface while the water droplet is pinned on the surfaces after UV irradiation (UV light, 365 nm, 30 mW cm^{-2}, 2 s; visible light, 530 nm, 20 mW cm^{-2}, 20 s). (b) Synthetic route of the fluorinated LLCP via ring-opening metathesis polymerization. M_n, number-average molecular weight. (c) Schematic illustrations of the electrospinning processing.

2.0) with a 2D detector of Pilatus3R in transmission mode ($q = 4\pi\sin\theta/\lambda$, where λ is the wavelength of 0.1542 nm and 2θ is the scattering angle). A Dataphysics OCA20 system was used to measure the CAs and SAs at ambient temperature in which 3 μL water droplets were used. In order to get a reliable value, the average CAs and SAs were obtained by measuring the same sample in at least five different positions. The light-controlled experiments were operated using 365 nm LED UV light (Omron, ZUV-C30H) and 530 nm LED visible light (CCS, HLV-24GR-3 W).

3 Results and discussion

3.1 Characterization of the LLCP

In order to manipulate the microscale water droplet ($\leq$ 4 μL), the fluorinated alkyl chain is incorporated to the end of side chain since fluorination is an effective strategy to lower the surface energy [31]. The fluorinated LLCP was synthesized via ring-opening metathesis polymerization (ROMP) with a high number-average molecular weight about 2.5 $\times$ 10^5 g mol^{-1} (Fig. 1b; please see Method for synthesis), which is at least one order of magnitude larger than that of the previously reported LCPs used for electrospinning. The LLCP was processed into the mats by electrospinning (Fig. 1c) and the detailed fabrication process is described in the Method section.

UV–vis spectroscopy was employed to investigate the photoisomerization of the LLCP (Figs 2a and 2b). Upon 365 nm UV light irradiation, the intensity of π-$\pi*$ transition band of *trans* isomer at 366 nm decreased; meanwhile, the n-$\pi*$ transition band of *cis* isomer at 444 nm gradually increased to photostationary state within 80 s. The reverse process was triggered by 530 nm light within 70 s. The change of the absorption bands indicates that the LLCP is able to undergo photoisomerization in response to UV and visible light. The mesomorphic properties of the LLCP were investigated by both DSC and POM equipped with a hot stage. As shown in Fig 2c, in the heating process, the LLCP exhibits glass transition at 31 °C and LC-isotropic phase transition (T_i) at 58 °C. Fig 2d shows the POM images of the LLCP obtained from the heating and cooling process. During heating, the schlieren textures was obviously observed at 25 °C and 35 °C, revealing the presence of the LC phase at room temperature. When the temperature was 60 °C ($>$ T_i), the textures disappeared because the LLCP underwent phase transition from LC to isotropic phase. During cooling, the LC textures appeared rapidly when the temperature was lower than T_i. 1D XRD experiments were performed to explore the LC structures of the fluorinated LLCP fiber at room temperature. As shown in Fig. 2e, the low-angle diffractions with a q-ratio of 1:$\sqrt{3}$ can be clearly observed, demonstrating the hexagonal packing. To further unveil the LC phase structure of the fluorinated LLCP, we carried out the 2D XRD experiments of fiber samples. As shown in Fig. 2f, when the X-ray incident beam is perpendicular to the fiber direction (z-axis), two low-angle diffraction peaks appear on the x-axis, indicating that the columns

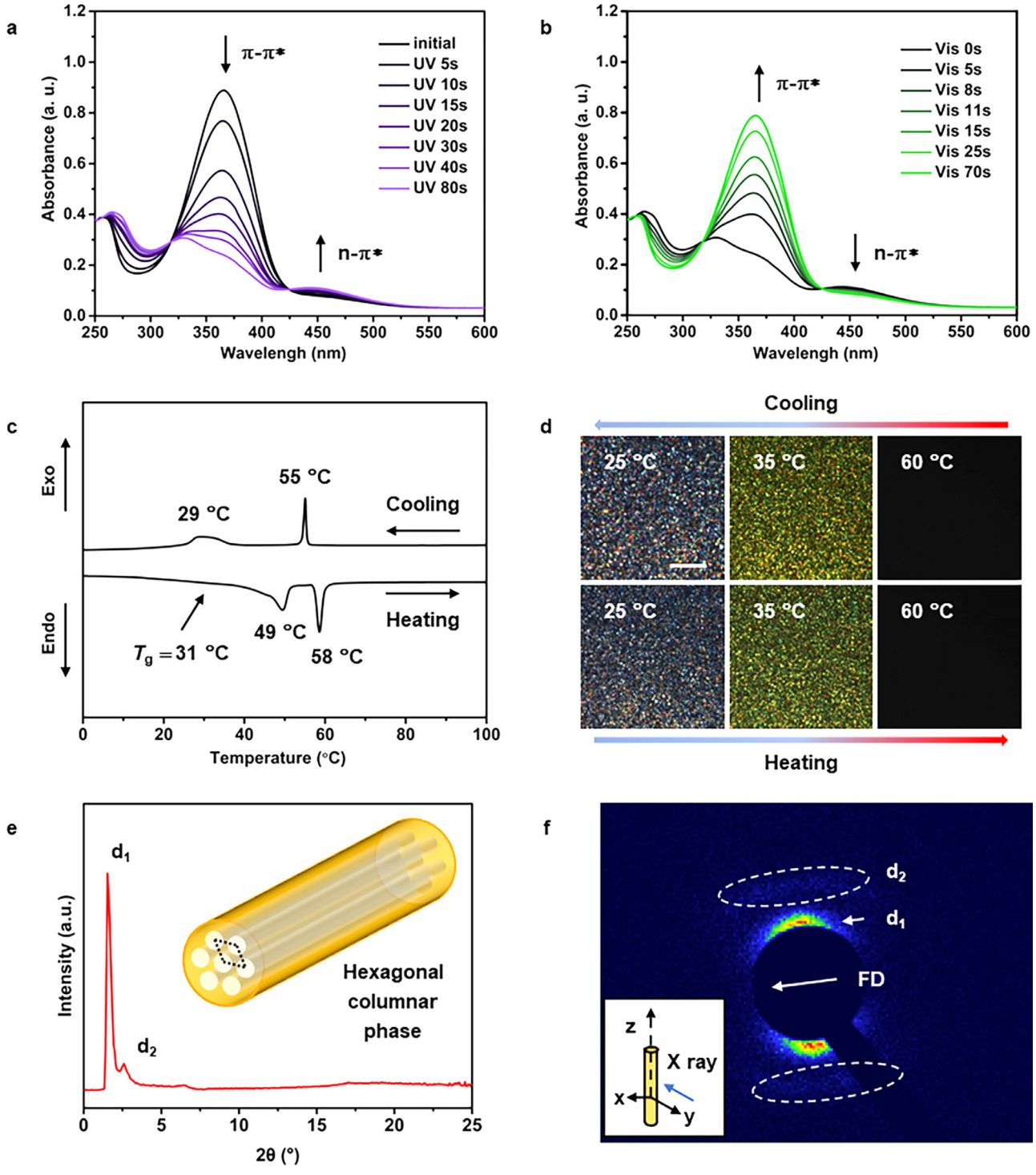

Fig. 2

(a,b) Changes in the UV–vis absorption spectra of the LLCP in dichloromethane solution (0.2 mg mL^{-1}) upon 365 nm light irradiation (30 mW cm^{-2}) (a) and then 530 nm light irradiation (50 mW cm^{-2}) (b). Black arrows indicate the trend in intensity change of π-$\pi*$ absorption band of the *trans*-azobenzene and n-$\pi*$ absorption band of the *cis*-azobenzene. (c) DSC curves of the LLCP upon heating and cooling. (d) POM images of the LLCP to show the textures at different temperature. Scale bars: 20 μm. (e) A 1D XRD pattern of the LLCP fiber recorded at room temperature. Inset, schematic illustration of the hexagonal columnar phase in the LLCP fiber. (f) 2D XRD patterns of the LLCP fiber recorded at room temperature. Inset, the X-ray beam was perpendicular to the fiber direction (along y-axis). FD, fiber direction.

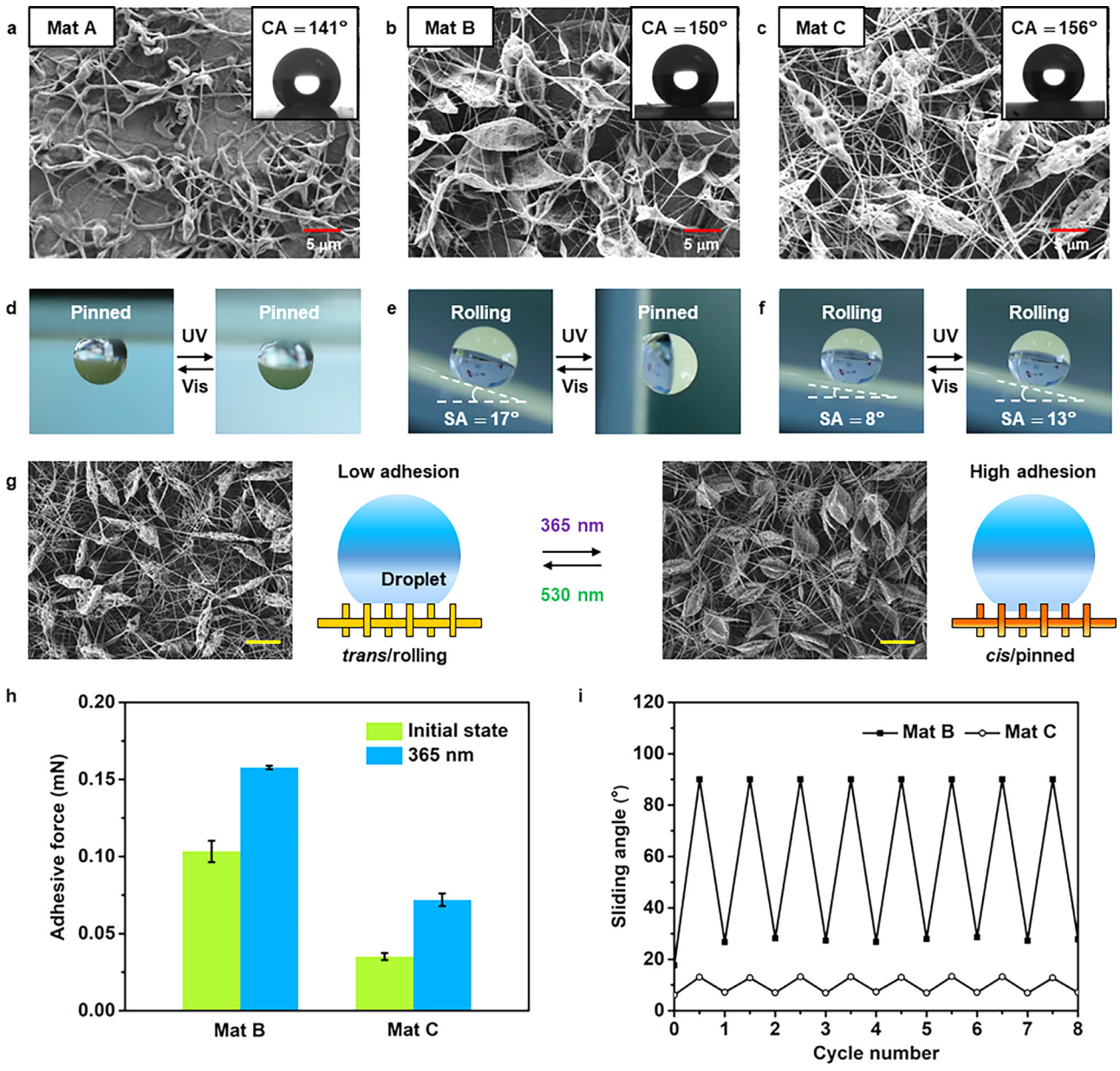

Fig. 3

(a–c) Representative SEM images of the fibers on LLCP mats electrospun from 0.5 wt% (Mat A) (a), 1 wt% (Mat B) (b), and 2 wt% (Mat C) (c) dichloromethane solution. All the fibers are continuous and randomly oriented. Insets show the profiles of the water droplet on the mats. CA, contact angle. (d-f) Microscopic profiles of the rolling and pinned water droplets. (d) The 3 μL water droplet is pinned on the Mat A at both *trans* and *cis* state. (e) The 3 μL water droplet rolls off from the Mat B at *trans* state and is pinned at *cis* state. (f) The 3 μL water droplet rolls off from the Mat C at both *trans* and *cis* state. SA, sliding angle. (g) SEM images and schematic illustration of the Mat B at different states upon light irradiation. (h) Photo-switchable adhesive force of the Mat B and the Mat C at the initial state and after UV irradiation. The direction of adhesive force is perpendicular to the mat surface. (i) Reversible changes of SAs on the superhydrophobic Mat B and Mat C for 8 cycles by sequential irradiation of UV and visible light. UV light, 365 nm, 30 mW cm^{-2}, 2 s; visible light, 530 nm, 20 mW cm^{-2}, 20 s.

of the hexagonal columnar phase are aligned parallel to the fiber direction.

3.2 Morphology and photo-switchable wettability of the LLCP mats

Because concentration has a significant influence on the morphology of the mat [32,33], three mats were electrospun from the dichloromethane solution with LLCP concentration of 0.5 wt% (Mat A), 1.0 wt% (Mat B), and 2 wt% (Mat C). The SEM images of three different electrospun mats are shown in Fig. 3a–c. It can be seen that the hederiform bumps spread all over the Mat A, while the Mat B and the Mat C are composed of nanofibers with many spindles, which contribute to the roughness of superhydrophobic surface. All the mats exhibit hydrophobic wettability with water CA above 140°. The Mat B and the Mat C containing more spindles even show superhydrophobicity with water CA of 150° and 156° (insets of Fig. 3a–c). In comparison with the flat LLCP substrate with a water CA of 110.3 ± 0.5°, the electrospun mats is more

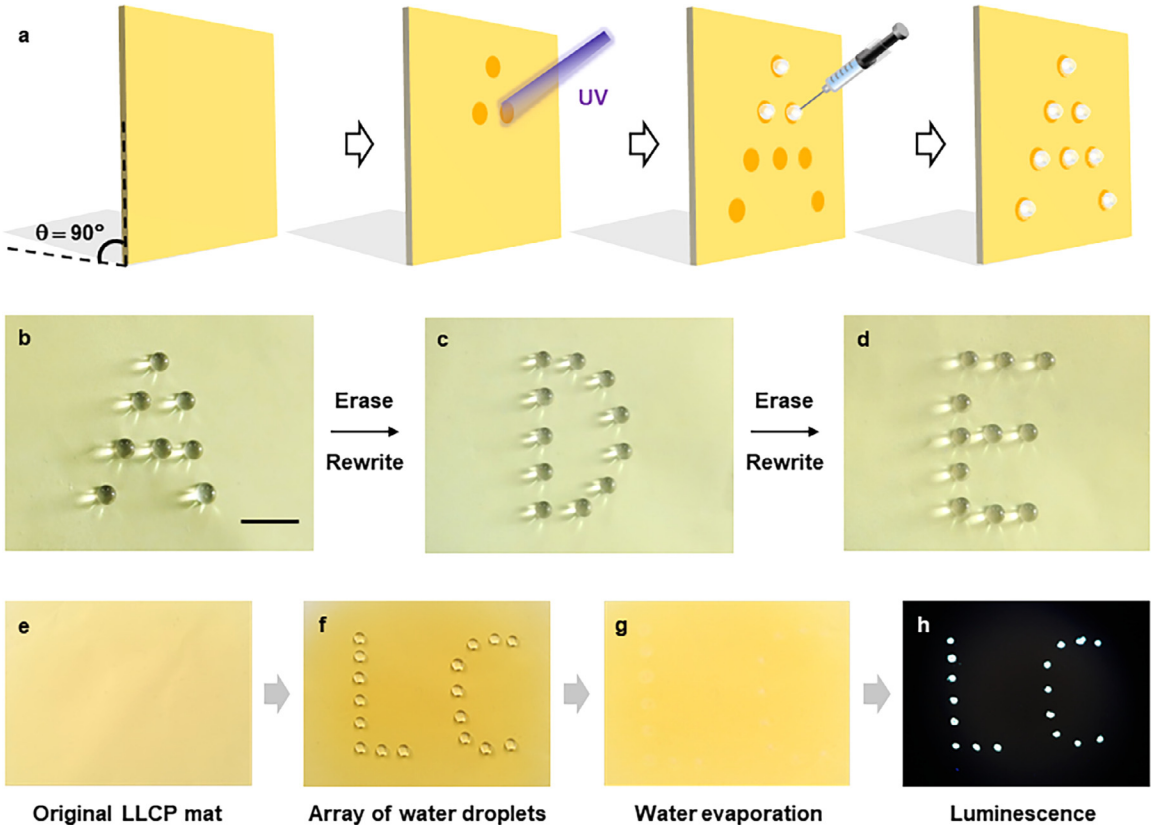

Fig. 4

(a) Schematic diagrams showing the procedure of light-directed pinning of the water droplets on the LLCP mat to form a pattern. (b-d) Photographs to show the different patterns of pinned water droplets on the LLCP mat. The 3 μL water droplets are pinned at the areas exposed to UV light. Scale bar: 5 mm. (e-h) Photographs to show the formation of fluorescent "LC"-shaped pattern on the LLCP mat. The water droplets containing aggregation-induced emission materials are pinned to form the "LC"-shaped array on the mat. After evaporation of the water droplets, the mat exhibits bright fluorescence upon faint UV irradiation to the same "LC" pattern. Size of the mat: 3 cm × 3 cm.

hydrophobic because of the hierarchical structure generated by the nanofibers on the surface. All three mats demonstrated a slight decrease of water CA value upon UV irradiation and then recovery after exposure to visible light due to the alteration of surface free energy aroused by reversible *trans-cis* isomerization of the azobenzene.

The SAs of the 3 μL water droplets on the different mats were carefully studied (Fig. 3d-e). A 3 μL water droplet was pinned on the Mat A, even when the LLCP mat was turned upside down. On the contrary, the 3 μL water droplets rolled off from the Mat B and the Mat C with SAs of 17° and 8°, respectively. After UV irradiation, the water droplet was still pinned on the Mat A and rolled off from the Mat C. Importantly, the Mat B showed the most distinguished change of SA from 16° to above 90°, i.e. a 3 μL droplet was pinned on the surface after UV irradiation. The SEM images and schematic illustration of the Mat B at different states are shown in Fig. 3g. Before UV irradiation, the assumed mode is that the water droplets rides only on the extreme top portions of the nanofibers whose microstructures provide sufficient roughness for the superhydrophobicity and low adhesive force. After UV irradiation, the Mat B remains the nanofibers with many spindles responsible for the superhydrophobicity. However, the *trans-cis* photoisomerization of azobenzene groups increases the surface polarity (the dipole moment of *cis* isomer is larger than that of *trans* isomer) and gives rise to the variation in the LC order [29]. In this case, the LLCP surface can only hold small amounts of air among the microstructures and result in relatively large adhesion, which is verified by the measurement of adhesive force. As Fig. 3h shows, both AF of the Mat B and the Mat C increases after UV irradiation. Corresponding to the differences of SA, AF of the Mat B increases from 0.11 to 0.16 mN, leading to the pinning of 3 μL water droplet on the surface. Although AF of the Mat C also increases from 0.03 to 0.07 mN, the enhanced AF is not enough for the Mat C to pin the water droplets. Subsequently, after visible light irradiation for 60 s, the AF value of the Mat B and the Mat C recovered to the initial state and the SAs changed to 22° and 8°, respectively. Such reversible switch of superhydrophobic adhesion is well retained after several cycles by alternative UV and visible light irradiation (Fig. 3i).

Compared to our previous work that reports the photo-induced pinning of 6 μL water droplets [29], smaller water droplets (3 μL) was manipulated on the Mat B because of the incorporation of low-surface-energy fluorinated alkyl chains to the LLCP. Uchida and Nakamura et al. also reported photo-switchable superhydrophobic adhesion by controlling the crystallization of diarylethene microcrystalline at different temperatures on

the surface; however, the switch between two wetting states took several hours or even one day [34]. By using the photoisomerization of azobenzene as well as the cooperative effect of LCs, the switch time for superhydrophobic adhesion change of our LLCP mat is much faster and only needs several seconds.

3.3 Light-directed pinning of small water droplets

The photo-switchable superhydrophobic adhesion of the Mat B provides a promising surface to dynamically manipulate the water droplets. Based on this feature, precise control of the water droplet array was realized on the vertically placed Mat B with a slant angle of 90°, which is greatly larger than that of 20° reported in the previous literature [29]. As shown in Fig. 4a, we fabricated patterns of high adhesive areas on the Mat B by using localized UV light irradiation. After UV irradiation, the selectively exposed regions became high adhesive in which the 3 μL water droplets were pinned to form desired arrays, while the unexposed areas remained the original low adhesion. Moreover, the existing pattern was able to be erased by 530 nm light irradiation and another different pattern could be created by the same method. Therefore, diverse arrays of water droplets, such as "A", "D", and "E"-shaped array, are obtained on the Mat B in sequence (Fig. 4b-d), which also suggests that the superhydrophobicity of the surface still remain the same after pinning and removing of 3 μL small water droplets for several times.

To demonstrate the practical value of the water droplet patterns on the surface, we further integrated the water-soluble aggregation induced emission (AIE) compound to support the programmable arrays (Figs 4e-h). The AIE-containing water drop (3 μL) is pinned on the mats to form a "LC" pattern. After water evaporation, the residual colorless AIE compound is concentrated in a small point and cannot be recognized by the naked eyes. When the mat is exposed faint UV light, the residual on the LLCP mat emits bright fluorescence to display the "LC" pattern.

4 Conclusions

In conclusion, superhydrophobic LLCP mats with photo-switchable adhesion were fabricated from fluorinated LLCP by electrospinning. Owing to the surface chemistry and microstructures, the LLCP mat with appropriate spindles exhibited superhydrophobicity with low adhesion similar to the case of lotus state, while the UV exposed mat shows the high water-adhesion characteristic, which can be favorably compared to that of the petal state. The well-known *trans-cis* isomerization of azobenzene cause significant change of the dipole moment and subsequently the variation of surface free energy, leading to the superhydrophobic adhesion change of the electrospun mats within seconds. We demonstrated the modulation of 3 μL water droplets on the LLCP mat, which is the smallest volume of water droplets, to our knowledge, that can be controlled by the LCP system. On the basis of photo-switchable wettability, diverse water droplet arrays were formed on the vertically placed mat in sequence by localized UV and visible irradiation, suggesting that the hierarchical structures remained intact with good fatigue resistance. Besides, the water-soluble AIE compound was exploited to further demonstrate the application in anti-counterfeiting technology. This feature to control interfacial properties on-demand of the LLCP mat will open up opportunities in numerous applications, including multiple controllable switches, microdroplets manipulation and so on.

Declaration of Competing Interest

The authors declare that they have no known competing financial interests or personal relationships that could have appeared to influence the work reported in this paper.

Acknowledgements

This work was financially supported by the National Natural Science Foundation of China (Grant Nos. 21734003, 51927805, 51721002) and Innovation Program of Shanghai Municipal Education Commission (2017–01–07–00–07-E00027).

References

[1] M. Liu, S. Wang, L. Jiang, Nature-inspired superwettability systems, Nat. Rev. Mater. 2 (2017) 17036, doi:10.1038/natrevmats.2017.36.

[2] V. Zorba, E. Stratakis, M. Barberoglou, E. Spanakis, P. Tzanetakis, S.H. Anastasiadis, C. Fotakis, Biomimetic artificial surfaces quantitatively reproduce the water repellency of a lotus leaf, Adv. Mater. 20 (2008) 4049–4054, doi:10.1002/adma.200800651.

[3] J.J. Li, Y.N. Zhou, Z.H. Luo, Polymeric materials with switchable superwettability for controllable oil/water separation: a comprehensive review, Prog. Polym. Sci. 87 (2018) 1–33, doi:10.1016/j.progpolymsci.2018.06.009.

[4] K. Nagata, T. Kurebayashi, K. Imato, N. Takeda, Photoresponsive fiber scaffolds with a core–sheath nanostructure for regulating cell behaviors, J. Mater. Chem. B 6 (2018) 2052–2056, doi:10.1039/c8tb00469b.

[5] Y. Zhao, Q. Lu, D. Chen, Y. Wei, Superhydrophobic modification of polyimide films based on gold-coated porous silver nanostructures and self-assembled monolayers, J. Mater. Chem. 16 (2006) 4504–4509, doi:10.1039/b608981j.

[6] Q. Fu, G.V.R. Rao, S.B. Basame, D.J. Keller, K. Artyushkova, J.E. Fulghum, G.P. López, Reversible control of free energy and topography of nanostructured surfaces, J. Am. Chem. Soc. 126 (2004) 8904–8905, doi:10.1021/ja047895q.

[7] T. Sun, G. Wang, L. Feng, B. Liu, Y. Ma, L. Jiang, D. Zhu, Reversible switching between superhydrophilicity and superhydrophobicity, Angew. Chem. Int. Ed. 43 (2004) 357–360, doi:10.1002/anie.200352565.

[8] D. Zhang, Z. Cheng, H. Kang, J. Yu, Y. Liu, L. Jiang, A smart superwetting surface with responsivity in both surface chemistry and microstructure, Angew. Chem. Int. Ed. 57 (2018) 3701–3705, doi:10.1002/anie.201800416.

[9] Y. Fu, B. Jin, Q. Zhang, X. Zhan, F. Chen, PH-induced switchable superwettability of efficient antibacterial fabrics for durable selective oil/water separation, ACS Appl. Mater. Interfaces 9 (2017) 30161–30170, doi:10.1021/acsami.7b09159.

[10] J.J. Li, Y.N. Zhou, Z.D. Jiang, Z.H. Luo, Electrospun fibrous mat with pH-switchable superwettability that can separate layered oil/water mixtures, Langmuir 32 (2016) 13358–13366, doi:10.1021/acs.langmuir.6b03627.

[11] B. Xin, J. Hao, Reversibly switchable wettability, Chem. Soc. Rev. 39 (2010) 769–782, doi:10.1039/b913622c.

[12] C. Gaillard, G. Cellot, S. Li, F.M. Toma, H. Dumortier, G. Spalluto, B. Cacciari, M. Prato, L. Ballerini, A. Bianco, Carbon nanotubes carrying cell-adhesion peptides do not interfere with neuronal functionality, Adv. Mater. 21 (2009) 2903–2908, doi:10.1002/adma.200900050.

[13] X. Qing, J.A. Lv, Y. Yu, Photodeformable liquid crystal polymers, Acta. Polym. Sin. 11 (2017) 1679–1705, doi:10.11777/j.issn1000-3304.2017.17196.

[14] Y. Zhan, Y. Liu, J. Lv, Y. Zhao, Y. Yu, Photoresponsive surfaces with controllable wettability, Prog. Chem. 27 (2015) 157–167, doi:10.7536/PC140821.

[15] K. Ichimura, S.K. Oh, M. Nakagawa, Light-driven motion of liquids on a photoresponsive surface, Science 288 (2000) 1624–1626, doi:10.1126/science.288.5471.1624.

[16] C. Li, Y. Zhang, J. Ju, F. Cheng, M. Liu, L. Jiang, Y. Yu, In situ fully light-driven switching of superhydrophobic adhesion, Adv. Funct. Mater. 22 (2012) 760–763, doi:10.1002/adfm.201101922.

[17] C. Zong, M. Hu, U. Azhar, X. Chen, Y. Zhang, S. Zhang, C. Lu, Smart copolymer-functionalized flexible surfaces with photoswitchable wettability: from superhydrophobicity with "rose petal" effect to superhydrophilicity, ACS Appl. Mater. Interfaces 11 (2019) 25436–25444, doi:10.1021/acsami.9b07767.

[18] F. Gao, Y. Yao, W. Wang, X. Wang, L. Li, Q. Zhuang, S. Lin, Light-driven transformation of bio-inspired superhydrophobic structure via reconfigurable PAzoMA microarrays: from lotus leaf to rice leaf, Macromolecules 51 (2018) 2742–2749, doi:10.1021/acs.macromol.8b00059.

[19] W. Jiang, G. Wang, Y. He, X. Wang, Y. An, Y. Song, L. Jiang, Photo-switched wettability on an electrostatic self-assembly azobenzene monolayer, Chem. Commun. (2005) 3550–3552, doi:10.1039/b504479k.

[20] H.S. Lim, J.T. Han, D. Kwak, M. Jin, K. Cho, Photoreversibly switchable superhydrophobic surface with erasable and rewritable pattern, J. Am. Chem. Soc. 128 (2006) 14458–14459, doi:10.1021/ja0655901.

[21] X. Hong, X. Gao, L. Jiang, Application of superhydrophobic surface with high adhesive force in no lost transport of superparamagnetic microdroplet, J. Am. Chem. Soc. 129 (2007) 1478–1479, doi:10.1021/ja065537c.

[22] Y. Zhan, J. Zhao, W. Liu, B. Yang, J. Wei, Y. Yu, Biomimetic submicroarrayed cross-linked liquid crystal polymer films with different wettability via colloidal lithography, ACS Appl. Mater. Interfaces 7 (2015) 25522–25528, doi:10.1021/acsami.5b09013.

[23] J.A. Lv, Y. Liu, J. Wei, E. Chen, L. Qin, Y. Yu, Photocontrol of fluid slugs in liquid crystal polymer microactuators, Nature 537 (2016) 179–184, doi:10.1038/nature19344.

[24] Y. Yu, M. Nakano, T. Ikeda, Directed bending of a polymer film by light, Nature 425 (2003) 145, doi:10.1038/425145a.

[25] X. Pang, J. an Lv, C. Zhu, L. Qin, Y. Yu, Photodeformable azobenzene-containing liquid crystal polymers and soft actuators, Adv. Mater. 31 (2019) 1–26, doi:10.1002/adma.201904224.

[26] T.J. White, D.J. Broer, Programmable and adaptive mechanics with liquid crystal polymer networks and elastomers, Nat. Mater. 14 (2015) 1087–1098, doi:10.1038/nmat4433.

[27] C. Li, F. Cheng, J.A. Lv, Y. Zhao, M. Liu, L. Jiang, Y. Yu, Light-controlled quick switch of adhesion on a micro-arrayed liquid crystal polymer superhydrophobic film, Soft Matter 8 (2012) 3730–3733, doi:10.1039/c2sm07471k.

[28] B. Xu, C. Zhu, L. Qin, J. Wei, Y. Yu, Light-directed liquid manipulation in flexible bilayer microtubes, Small 15 (2019) 1–6, doi:10.1002/smll.201901847.

[29] Y. Liu, C. Zhu, Y. Zhao, X. Qing, F. Wang, D. Deng, J. Wei, Y. Yu, Directed pinning of moving water droplets on photoresponsive liquid crystal mats, Adv. Mater. Interfaces 6 (2019) 1–7, doi:10.1002/admi.201901158.

[30] J.A. Lv, W. Wang, W. Wu, Y. Yu, A reactive azobenzene liquid-crystalline block copolymer as a promising material for practical application of light-driven soft actuators, J. Mater. Chem. C 3 (2015) 6621–6626, doi:10.1039/c5tc00595g.

[31] A.F. Thünemann, Complexes of polyethyleneimine with perfluorinated carboxylic acids: wettability of lamellar structured mesophases, Langmuir 16 (2000) 824–828, doi:10.1021/la9907026.

[32] C. Huang, S.J. Soenen, J. Rejman, B. Lucas, K. Braeckmans, J. Demeester, S.C. de Smedt, Stimuli-responsive electrospun fibers and their applications, Chem. Soc. Rev. 40 (2011) 2417–2434, doi:10.1039/c0cs00181c.

[33] Y. Chen, H. Kim, Preparation of superhydrophobic membranes by electrospinning of fluorinated silane functionalized poly(vinylidene fluoride), Appl. Surf. Sci. 255 (2009) 7073–7077, doi:10.1016/j.apsusc.2009.03.043.

[34] K. Uchida, N. Nishikawa, N. Izumi, S. Yamazoe, H. Mayama, Y. Kojima, S. Yokojima, S. Nakamura, K. Tsujii, M. Irie, Phototunable diarylethene microcrystalline surfaces: Lotus and petal effects upon wetting, Angew. Chem. Int. Ed. 49 (2010) 5942–5944, doi:10.1002/anie.201000793.